

# LANTERN++: ENHANCED RELAXED SPECULATIVE DECODING WITH STATIC TREE DRAFTING FOR VISUAL AUTO-REGRESSIVE MODELS

Sihwan Park<sup>1\*</sup> Doohyuk Jang<sup>1\*</sup> Sungyub Kim<sup>1</sup> Souvik Kundu<sup>2</sup> Eunho Yang<sup>1,3†</sup>

<sup>1</sup>KAIST <sup>2</sup>Intel Labs <sup>3</sup>AITRICS

{sihwan.park, jadohu, eunhoy}@kaist.ac.kr

souvik.kundu@intel.com sungyub.kim@mli.kaist.ac.kr

## ABSTRACT

Speculative decoding has been widely used to accelerate autoregressive (AR) text generation. However, its effectiveness in visual AR models remains limited due to token selection ambiguity, where multiple tokens receive similarly low probabilities, reducing acceptance rates. While dynamic tree drafting has been proposed to improve speculative decoding, we show that it fails to mitigate token selection ambiguity, resulting in shallow draft trees and suboptimal acceleration. To address this, we introduce LANTERN++, a novel framework that integrates static tree drafting with a relaxed acceptance condition, allowing drafts to be selected independently of low-confidence predictions. This enables deeper accepted sequences, improving decoding efficiency while preserving image quality. Extensive experiments on state-of-the-art visual AR models demonstrate that LANTERN++ significantly accelerates inference, achieving up to  $\times 2.56$  speedup over standard AR decoding while maintaining high image quality.

## 1 INTRODUCTION

Recent advances in speculative decoding have significantly accelerated auto-regressive (AR) generation in language models (Leviathan et al., 2023; Cai et al., 2024; Li et al., 2024a;b). Extending this approach to visual AR models (Sun et al., 2024; Team, 2024; Chern et al., 2024; Liu et al., 2024) presents unique challenges due to the inherent nature of image token distributions. In particular, Jang et al. (2025) identified a key issue, *token selection ambiguity*, wherein multiple next-tokens receive nearly equivalent probabilities. This results in the drafter model struggling to accurately predict the next token, since even the target model itself lacks a highly confident choice. Consequently, speculative acceleration becomes ineffective as the drafter’s predictions tend to be unreliable.

LANTERN (Jang et al., 2025) addressed this by introducing a relaxed acceptance condition leveraging latent-space similarities, where tokens that are close in the latent space are treated as visually similar. This method improved inference speed while maintaining high image quality. However, LANTERN was implemented using EAGLE-2’s (Li et al., 2024b) *dynamic tree drafting*, which adaptively selects draft tokens based on the drafter’s confidence. In visual AR models, token selection ambiguity leads to two major issues in dynamic tree drafting: (1) low-confidence scores from the drafter result in excessively shallow draft trees, preventing the formation of long accepted sequences, and (2) draft tokens are deterministically selected based on drafter confidence, leading to overly low acceptance probabilities. These two factors collectively degrade the overall efficiency of speculative decoding.

To overcome these limitations, we introduce *LANTERN++*, an enhanced framework that revises two key aspects: (1) the adoption of *static tree drafting* and (2) the integration of a *multiplicative bound* tailored to static tree drafting. By employing static tree drafting, LANTERN++ ensures that deep draft sequences can be generated even under low-confidence conditions. Moreover, static tree drafting allows draft tokens to be selected stochastically rather than deterministically based on confidence,

\*Equal Contribution

†Corresponding Author



Figure 1: Images generated by LANTERN++ on Lumina-mGPT exhibit remarkable acceleration in decoding steps while maintaining high generation quality. The top row shows images generated by standard auto-regressive decoding, while the bottom row displays images generated with acceleration through LANTERN++. The step compression ratio is presented in white at the bottom-right of each image.

effectively restoring a normal level of acceptance probability. Additionally, LANTERN++ refines the relaxation mechanism by replacing the additive acceptance boost with a multiplicative distributional distortion bound, which scales acceptance probabilities relative to the original distribution. This adjustment prevents disproportionate favoring of certain tokens, ensuring stable probability scaling and preserving distributional consistency. Extensive experiments demonstrate that LANTERN++ achieves substantial speedups while maintaining high image quality, making it a promising direction for efficient visual AR modeling.

Our main contributions are as follows:

- We analyze dynamic vs. static tree drafting in speculative decoding and show that static tree drafting enables longer accepted sequences by removing confidence-based constraints.
- We introduce **LANTERN++**, which integrates static tree drafting with a multiplicative relaxation mechanism to ensure stable and consistent acceptance probabilities.
- Extensive experiments demonstrate that LANTERN++ achieves up to  $\times 2.56$  lower latency and  $\times 3.63$  step compression while maintaining high image quality.

## 2 PRELIMINARIES

**Notations** We define the *target model* as the visual AR model being accelerated and the *drafter model* as the auxiliary model generating draft tokens. The drafter and target models define probability distributions  $p(\cdot|s)$  and  $q(\cdot|s)$  where  $s$  is the preceding sequence, respectively. Individual tokens are denoted as lowercase  $x$  and sequences as uppercase  $X$  (e.g.,  $X_{i:j} = (x_i, \dots, x_j)$ ).

**Tree Drafting and Verification** Unlike standard chain drafting (Leviathan et al., 2023), which generates a single draft token sequence, tree drafting (Cai et al., 2024; Li et al., 2024a;b) samples multiple draft tokens per forward pass, forming a tree structure for diverse draft sequences. Given an input  $X_{1:N}$ , the drafter first samples  $s_1$  tokens  $\hat{x}_{1,1}, \dots, \hat{x}_{1,s_1}$  from  $p(x|X_{1:N})$ , then expands each token with  $s_2$  subsequent drafts in a single forward pass using a tree-aware attention mask. This process continues up to depth  $K$ , constructing a draft tree with only  $K$  forward passes. The tree is then flattened and verified by the target model in a single forward pass.

Tree drafting has two main variants. *Static tree drafting* (Cai et al., 2024; Li et al., 2024a) uses a fixed tree structure where a predefined set of draft tokens are generated at each level. *Dynamic tree drafting* (Li et al., 2024b) adapts the tree structure based on context. It estimates a global accept probability for each token as  $\bar{V}_i = \prod_{t_j \in \text{Path}(\text{root}, t_i)} p_j \approx \prod_{t_j \in \text{Path}(\text{root}, t_i)} c_j$ , where  $p_j$  is the actual

Table 1: Step compression ratios of static (EAGLE-1) and dynamic (EAGLE-2) tree drafting across different modalities. Dynamic tree drafting improves compression in language models (Vicuna-7B (Zheng et al., 2023)) but performs worse than static tree drafting in visual AR models (LlamaGen-3B (Sun et al., 2024)) due to token selection ambiguity.

| Methods                         | Step Compression Ratio |                        |
|---------------------------------|------------------------|------------------------|
|                                 | LlamaGen-3B            | Vicuna-7B              |
| EAGLE-1 (Static Tree Drafting)  | $\times 2.49$          | $\times 3.94$          |
| EAGLE-2 (Dynamic Tree Drafting) | $\times 2.11$ (-15.3%) | $\times 4.98$ (+26.4%) |

accept probability and  $c_j$  is the drafter’s confidence score. The model then expands the top- $k$  tokens and trims the set of drafts by  $V_i$  before verification.

**Token Selection Ambiguity and LANTERN** Visual AR models exhibit *token selection ambiguity* (Jang et al., 2025), where next-token distributions are more dispersed than in language models (Brown et al., 2020; Touvron et al., 2023; Jiang et al., 2023), resulting in the drafter often failing to predict the target model’s outputs accurately and thus limiting the overall speedup achievable via speculative decoding. To address this, LANTERN (Jang et al., 2025) exploits latent proximity by treating visually similar (close in latent space) tokens as interchangeable. Given a draft token  $\tilde{x}$ , it identifies its  $k$  nearest neighbors in latent space,  $B_k(\tilde{x})$ , and applies a Total Variation Distance (TVD) constraint  $\delta > 0$  to refine the neighborhood into  $A_{k,\delta}(\tilde{x})$ , ensuring minimal distributional distortion. The acceptance condition is then relaxed from  $\min(1, \frac{q(\tilde{x}|s)}{p(\tilde{x}|s)})$  to  $\min\left(1, \sum_{x \in A_{k,\delta}(\tilde{x})} \frac{q(x|s)}{p(\tilde{x}|s)}\right)$ , boosting the effective acceptance rate while preserving image quality. Additional preliminaries are provided in Appendix A.

### 3 WHY DYNAMIC TREE DRAFTING FAILS IN VISUAL AR MODELS

Applying dynamic tree drafting to visual AR models, where token selection ambiguity is prevalent, introduces two key issues: (1) draft trees become overly shallow due to low drafter confidence, and (2) the deterministic selection of draft tokens results in consistently low acceptance probabilities. These factors fundamentally limit the effectiveness of speculative decoding by restricting the acceptance of longer draft sequences, thereby reducing overall acceleration.

**Shallow Draft Tree.** Dynamic tree drafting computes a global accept probability for each draft node in the draft tree as the product of the drafter’s confidence scores along the path from the root:  $V_i = \prod_{t_j \in \text{Path}(\text{root}, t_i)} c_j$ . However, in visual AR models, where drafter confidence scores tend to be low, this product decays exponentially as draft sequence length increases. Consequently, longer draft sequences become significantly less likely to survive, leaving only shorter ones. The result is a draft tree that is wide (many branches) but shallow, preventing the formation of long accepted sequences. Since longer sequences are key to achieving high step compression, this structural limitation fundamentally restricts the acceleration potential of dynamic tree drafting. An example resulting shallow tree can be found in Appendix C.1.

**Low Accept Probabilities.** In speculative sampling (Leviathan et al., 2023), a draft token  $\tilde{x}$  is accepted with probability  $\min(1, q(\tilde{x}|s)/p(\tilde{x}|s))$ , which depends on the alignment between the drafter’s predictions and the target model’s likelihood. However, in dynamic tree drafting, tokens are deterministically selected based on the drafter’s confidence, effectively setting  $p(\tilde{x}|s) = 1$ . This reduces the acceptance probability to  $q(\tilde{x}|s)$ . Due to token selection ambiguity, visual AR models produce highly dispersed next-token distributions, with even the most likely token often receiving a probability below 0.2. As a result, even accurate drafter predictions lead to an unnecessarily low acceptance rate.

Table 1 highlights the contrasting effects of dynamic tree drafting in language models and visual AR models. In language models, dynamic tree drafting improves the step compression ratio from  $\times 3.94$  to  $\times 4.98$ , leveraging concentrated next-token distributions and high-confidence drafter predictions to construct deeper draft trees. In visual AR models, however, token selection ambiguity leads to

dispersed next-token distributions and lower drafter confidence, producing wide yet shallow draft trees. Consequently, static tree drafting achieves a higher step compression ratio ( $\times 2.49$ ) than dynamic tree drafting ( $\times 2.11$ ), underscoring the latter’s limitations in handling token selection ambiguity.

#### 4 LANTERN++: RELAXED ACCEPTANCE WITH STATIC TREE DRAFTING

As demonstrated in Section 3, dynamic tree drafting in visual AR models suffers from limited tree depth and low accept probabilities due to token selection ambiguity. Static tree drafting, in contrast, avoids these pitfalls by relying on a fixed tree structure rather than confidence-based path selection. However, it still struggles with low accept probabilities, as visual AR models inherently assign low probabilities to individual tokens. To address this, we introduce **LANTERN++**, a refined relaxation of the acceptance condition tailored for static tree drafting.

A key challenge in applying relaxation methods to static tree drafting is the variability of  $p(x|s)$ . Unlike dynamic tree drafting, where draft tokens are deterministically selected ( $p(x|s) = 1$ ), static tree drafting maintains the true drafter probabilities, which can vary significantly across tokens. This variability makes the original additive relaxation strategy problematic: when  $p(x|s)$  is small, an additive increase  $\delta$  can lead to disproportionately high accept probabilities, while for larger  $p(x|s)$ , the boost becomes negligible. This lack of proportionality results in inconsistent behavior and potential distortion of the target distribution.

To overcome this issue, LANTERN++ replaces the additive relaxation with a *multiplicative distributional distortion bound*  $\lambda$ , ensuring that accept probability adjustments remain proportional to the target model’s likelihood. Specifically, for each draft token  $\hat{x}$ , its neighborhood  $B_k(\hat{x})$  is first determined in the same manner as in LANTERN. A refined subset  $A_{k,\lambda}(\hat{x}) \subseteq B_k(\hat{x})$  is then selected such that

$$\sum_{x \in A_{k,\lambda}(\hat{x})} q(x|s) < \lambda q(\hat{x}|s),$$

where  $\lambda > 1$  is a predefined constant. This ensures that the aggregated target probability does not exceed  $\lambda$  times the original likelihood  $q(\hat{x}|s)$  (and thus guarantees that the relaxed accept probability does not exceed  $\lambda$  times the original accept probability). The final accept probability is then given by:

$$\min \left( 1, \sum_{x \in A_{k,\lambda}(\hat{x})} \frac{q(x|s)}{p(\hat{x}|s)} \right).$$

This multiplicative relaxation offers two key advantages. First, it maintains a *consistent proportional adjustment* across different values of  $p(\hat{x}|s)$ , ensuring that the acceptance probability is neither excessively inflated nor suppressed. Second, it prevents *instability in cases where  $p(\hat{x}|s)$  is small*, as a fixed additive boost could lead to over-amplification. By contrast, the multiplicative bound scales naturally with  $q(x|s)$ , yielding a more stable and controlled relaxation.

In summary, LANTERN++ refines the acceptance condition for static tree drafting by introducing a multiplicative bound that maintains proportionality and stability. This adjustment leads to a more predictable relaxation mechanism, improved alignment with the target distribution, and better acceleration performance in visual AR models.

#### 5 EXPERIMENTS

We conduct extensive experiments to evaluate the effectiveness of LANTERN++ in accelerating inference for visual AR models while preserving image quality. Our evaluation compares LANTERN++ against standard autoregressive (AR) decoding and EAGLE-1 (Li et al., 2024a) across multiple state-of-the-art visual AR models, including Lumina-mGPT (Liu et al., 2024), Anole (Chern et al., 2024), and LlamaGen-XL (Sun et al., 2024). All experiments are conducted on the MS-COCO 2017 validation set (Lin et al., 2014) using a single NVIDIA A100 PCIe 80GB GPU. More details on the experimental setting can be found in Appendix B.

Table 2 presents the step compression ratios and inference latency of each method. LANTERN++ consistently outperforms EAGLE-1 across all models, achieving higher step compression and lower

Table 2: Acceleration performance and image generation performance of standard decoding, EAGLE-1, and LANTERN++ over different visual AR models on MS-COCO 2017 validation captions.

| Method                                   | MS-COCO 2017 Validation (Lin et al., 2014) |                        |                      |                           |
|--|--|------------------------|----------------------|---------------------------|
|  | Acceleration ( $\uparrow$ )                |                        | Image Quality        |                           |
|  | Steps                                      | Latency                | FID ( $\downarrow$ ) | CLIP Score ( $\uparrow$ ) |
| Lumina-mGPT (Liu et al., 2024)           | $\times 1.00$                              | $\times 1.00$          | 28.93                | 0.3333                    |
| EAGLE-1 (Li et al., 2024a)               | $\times 2.94$                              | $\times 2.10$          | 29.22                | 0.3325                    |
| LANTERN++ ( $k = 10, \lambda = 2$ )      | $\times 3.19$                              | $\times 2.28$          | 30.11                | 0.3296                    |
| LANTERN++ ( $k = 10, \lambda = 3$ )      | $\times \mathbf{3.63}$                     | $\times \mathbf{2.56}$ | 33.91                | 0.3267                    |
| Anole (Chern et al., 2024)               | $\times 1.00$                              | $\times 1.00$          | 20.28                | 0.3215                    |
| EAGLE-1                                  | $\times 2.68$                              | $\times 1.75$          | 20.22                | 0.3206                    |
| LANTERN++ ( $k = 10, \lambda = 2$ )      | $\times 2.95$                              | $\times 1.85$          | 21.10                | 0.3201                    |
| LANTERN++ ( $k = 10, \lambda = 3$ )      | $\times \mathbf{3.41}$                     | $\times \mathbf{2.21}$ | 25.48                | 0.3164                    |
| LlamaGen-XL (Stage I) (Sun et al., 2024) | $\times 1.00$                              | $\times 1.00$          | 23.64                | 0.3162                    |
| EAGLE-1                                  | $\times 2.50$                              | $\times 1.90$          | 23.64                | 0.3162                    |
| LANTERN++ ( $k = 10, \lambda = 3$ )      | $\times \mathbf{2.98}$                     | $\times \mathbf{2.15}$ | 23.89                | 0.3159                    |
| LlamaGen-XL (Stage II)                   | $\times 1.00$                              | $\times 1.00$          | 40.52                | 0.2920                    |
| EAGLE-1                                  | $\times 2.38$                              | $\times 1.83$          | 40.71                | 0.2925                    |
| LANTERN++ ( $k = 10, \lambda = 3$ )      | $\times \mathbf{2.86}$                     | $\times \mathbf{2.14}$ | 39.80                | 0.2927                    |

Figure 2: Images generated by LANTERN++ on Lumina-mGPT with average step compression ratio  $\times 3.63$ . The top row shows images generated by standard auto-regressive decoding, and the bottom row displays images generated with acceleration through LANTERN++.

latency. Notably, on Lumina-mGPT, LANTERN++ improves the step compression ratio from  $\times 2.94$  to  $\times 3.63$ , reducing latency from  $\times 2.10$  to  $\times 2.56$ . Similar trends are observed for Anole ( $\times 3.41$  vs.  $\times 2.68$ ) and LlamaGen-XL Stage 2 ( $\times 2.86$  vs.  $\times 2.38$ ). These results demonstrate that LANTERN++ enables deeper accepted sequences by decoupling token selection from low-confidence predictions, leading to greater acceleration.

In addition to efficiency, we assess the impact of LANTERN++ on image quality using Fréchet Inception Distance (FID) (Heusel et al., 2017) and CLIP score (Hessel et al., 2021). While LANTERN++ slightly increases FID due to its relaxed acceptance condition, the overall degradation remains minimal. For example, on Lumina-mGPT, FID increases from 28.93 (standard AR) to 30.11 ( $\lambda = 2$ ) and 33.91 ( $\lambda = 3$ ), while maintaining a competitive CLIP score. This trade-off highlights the flexibility of LANTERN++ in balancing speed and quality by adjusting the multiplicative bound  $\lambda$ . To further assess visual fidelity, Figure 2 presents images generated by LANTERN++ vs. standard AR decoding on Lumina-mGPT. Despite the increased acceleration, the visual quality remains *highly consistent*, with no significant loss of detail or artifacts. This qualitative analysis aligns with the quantitative results, confirming that LANTERN++ maintains strong generation quality while substantially reducing inference time. More comprehensive experimental results are provided in Appendix C.

## 6 CONCLUSION

We introduced LANTERN++, a speculative decoding framework that significantly improves acceleration in visual AR models by addressing token selection ambiguity. Our analysis highlighted the limitations of dynamic tree drafting under token selection ambiguity, where deterministic token selection leads to shallow draft trees and overly conservative acceptance probabilities, reducing acceleration efficiency. By decoupling draft selection from low-confidence predictions, LANTERN++

enables deeper accepted sequences and more effective acceleration while maintaining high image quality. However, tuning the multiplicative bound remains crucial for balancing acceleration and image quality. Future work could explore adaptive acceptance mechanisms that dynamically adjust relaxation based on token uncertainty, as well as hybrid drafting strategies that combine the strengths of static and dynamic tree structures to further improve efficiency.

## REFERENCES

- Tom Brown, Benjamin Mann, Nick Ryder, Melanie Subbiah, Jared D Kaplan, Prafulla Dhariwal, Arvind Neelakantan, Pranav Shyam, Girish Sastry, Amanda Askell, Sandhini Agarwal, Ariel Herbert-Voss, Gretchen Krueger, Tom Henighan, Rewon Child, Aditya Ramesh, Daniel Ziegler, Jeffrey Wu, Clemens Winter, Chris Hesse, Mark Chen, Eric Sigler, Mateusz Litwin, Scott Gray, Benjamin Chess, Jack Clark, Christopher Berner, Sam McCandlish, Alec Radford, Ilya Sutskever, and Dario Amodei. Language models are few-shot learners. In H. Larochelle, M. Ranzato, R. Hadsell, M.F. Balcan, and H. Lin (eds.), *Advances in Neural Information Processing Systems*, volume 33, pp. 1877–1901. Curran Associates, Inc., 2020. URL [https://proceedings.neurips.cc/paper\\_files/paper/2020/file/1457c0d6bfc4967418bfb8ac142f64a-Paper.pdf](https://proceedings.neurips.cc/paper_files/paper/2020/file/1457c0d6bfc4967418bfb8ac142f64a-Paper.pdf).
- Tianle Cai, Yuhong Li, Zhengyang Geng, Hongwu Peng, Jason D. Lee, Deming Chen, and Tri Dao. Medusa: Simple LLM inference acceleration framework with multiple decoding heads. In *Forty-first International Conference on Machine Learning*, 2024. URL <https://openreview.net/forum?id=PEpbUobfJv>.
- Ethan Chern, Jiadi Su, Yan Ma, and Pengfei Liu. Anole: An open, autoregressive, native large multimodal models for interleaved image-text generation, 2024. URL <https://arxiv.org/abs/2407.06135>.
- Christoph Chuhmann, Andreas Köpf, Richard Vencu, Theo Coombes, and Romain Beaumont. Laion coco: 600m synthetic captions from laion2b-en, 2022. URL <https://laion.ai/blog/laion-coco/>. September 27th, 2024.
- Yichao Fu, Peter Bailis, Ion Stoica, and Hao Zhang. Break the sequential dependency of LLM inference using lookahead decoding. In *Forty-first International Conference on Machine Learning*, 2024. URL <https://openreview.net/forum?id=eDjvSFokXw>.
- Jack Hessel, Ari Holtzman, Maxwell Forbes, Ronan Le Bras, and Yejin Choi. CLIPScore: A reference-free evaluation metric for image captioning. In Marie-Francine Moens, Xuanjing Huang, Lucia Specia, and Scott Wen-tau Yih (eds.), *Proceedings of the 2021 Conference on Empirical Methods in Natural Language Processing*, pp. 7514–7528, Online and Punta Cana, Dominican Republic, November 2021. Association for Computational Linguistics. doi: 10.18653/v1/2021.emnlp-main.595. URL <https://aclanthology.org/2021.emnlp-main.595>.
- Martin Heusel, Hubert Ramsauer, Thomas Unterthiner, Bernhard Nessler, and Sepp Hochreiter. Gans trained by a two time-scale update rule converge to a local nash equilibrium. In I. Guyon, U. Von Luxburg, S. Bengio, H. Wallach, R. Fergus, S. Vishwanathan, and R. Garnett (eds.), *Advances in Neural Information Processing Systems*, volume 30. Curran Associates, Inc., 2017. URL [https://proceedings.neurips.cc/paper\\_files/paper/2017/file/8a1d694707eb0fe65871369074926d-Paper.pdf](https://proceedings.neurips.cc/paper_files/paper/2017/file/8a1d694707eb0fe65871369074926d-Paper.pdf).
- Jonathan Ho and Tim Salimans. Classifier-free diffusion guidance. In *NeurIPS 2021 Workshop on Deep Generative Models and Downstream Applications*, 2021. URL <https://openreview.net/forum?id=qw8AKxfYbI>.
- Doohyuk Jang, Sihwan Park, June Yong Yang, Yeonsung Jung, Jihun Yun, Souvik Kundu, Sung-Yub Kim, and Eunho Yang. Lantern: Accelerating visual autoregressive models with relaxed speculative decoding, 2025. URL <https://arxiv.org/abs/2410.03355>.
- Albert Q. Jiang, Alexandre Sablayrolles, Arthur Mensch, Chris Bamford, Devendra Singh Chaplot, Diego de las Casas, Florian Bressand, Gianna Lengyel, Guillaume Lample, Lucile Saulnier, L  lio Renard Lavaud, Marie-Anne Lachaux, Pierre Stock, Teven Le Scao, Thibaut Lavril, Thomas

- Wang, Timothée Lacroix, and William El Sayed. Mistral 7b, 2023. URL <https://arxiv.org/abs/2310.06825>.
- Yaniv Leviathan, Matan Kalman, and Yossi Matias. Fast inference from transformers via speculative decoding. In *International Conference on Machine Learning*, pp. 19274–19286. PMLR, 2023.
- Yuhui Li, Fangyun Wei, Chao Zhang, and Hongyang Zhang. Eagle: Speculative sampling requires rethinking feature uncertainty, 2024a.
- Yuhui Li, Fangyun Wei, Chao Zhang, and Hongyang Zhang. Eagle-2: Faster inference of language models with dynamic draft trees. *arXiv preprint arXiv:2406.16858*, 2024b.
- Tsung-Yi Lin, Michael Maire, Serge Belongie, James Hays, Pietro Perona, Deva Ramanan, Piotr Dollár, and C. Lawrence Zitnick. Microsoft coco: Common objects in context. In David Fleet, Tomas Pajdla, Bernt Schiele, and Tinne Tuytelaars (eds.), *Computer Vision – ECCV 2014*, pp. 740–755, Cham, 2014. Springer International Publishing. ISBN 978-3-319-10602-1.
- Dongyang Liu, Shitian Zhao, Le Zhuo, Weifeng Lin, Yu Qiao, Hongsheng Li, and Peng Gao. Lumina-mgpt: Illuminate flexible photorealistic text-to-image generation with multimodal generative pretraining, 2024. URL <https://arxiv.org/abs/2408.02657>.
- Ilya Loshchilov and Frank Hutter. Decoupled weight decay regularization. In *International Conference on Learning Representations*, 2019. URL <https://openreview.net/forum?id=Bkg6RiCqY7>.
- Peize Sun, Yi Jiang, Shoufa Chen, Shilong Zhang, Bingyue Peng, Ping Luo, and Zehuan Yuan. Autoregressive model beats diffusion: Llama for scalable image generation. *arXiv preprint arXiv:2406.06525*, 2024.
- Chameleon Team. Chameleon: Mixed-modal early-fusion foundation models. *arXiv preprint arXiv:2405.09818*, 2024.
- Hugo Touvron, Thibaut Lavril, Gautier Izacard, Xavier Martinet, Marie-Anne Lachaux, Timothée Lacroix, Baptiste Rozière, Naman Goyal, Eric Hambro, Faisal Azhar, Aurelien Rodriguez, Armand Joulin, Edouard Grave, and Guillaume Lample. Llama: Open and efficient foundation language models, 2023. URL <https://arxiv.org/abs/2302.13971>.
- Jiahui Yu, Yuanzhong Xu, Jing Yu Koh, Thang Luong, Gunjan Baid, Zirui Wang, Vijay Vasudevan, Alexander Ku, Yinfei Yang, Burcu Karagol Ayan, et al. Scaling autoregressive models for content-rich text-to-image generation. *arXiv preprint arXiv:2206.10789*, 2(3):5, 2022.
- Lianmin Zheng, Wei-Lin Chiang, Ying Sheng, Siyuan Zhuang, Zhanghao Wu, Yonghao Zhuang, Zi Lin, Zhuohan Li, Dacheng Li, Eric Xing, et al. Judging llm-as-a-judge with mt-bench and chatbot arena. *Advances in Neural Information Processing Systems*, 36:46595–46623, 2023.

## APPENDIX

## A ADDITIONAL PRELIMINARIES

## A.1 VISUAL AUTO-REGRESSIVE MODELING

In visual AR models, image generation involves two main stages: generating image tokens through auto-regression and decoding the image tokens into actual image patches. In a text-to-image generation setting, given a tokenized text prompt  $X_{1:N}$ , the model generates a sequence of image tokens  $X_{N+1:N+K}$  based on the following probability modeling:

$$P(X_{N+1:N+K} | X_{1:N}) = \prod_{\ell=1}^K P(x_{N+\ell} | X_{1:N+\ell-1}),$$

where  $K$  represents the total number of image tokens corresponding to the height and width of the image feature map. Since each token is predicted based solely on its preceding tokens, visual AR models require  $K$  sequential steps to generate all  $K$  image tokens.

Once the  $K$  image tokens are generated, they are mapped to visual representation by referring to the codebook  $\mathcal{C}$ . Specifically, the codebook  $\mathcal{C} = \{c_1, \dots, c_L\}$  consists of codes  $c_i \in \mathbb{R}^d$ , where each code is a latent feature used by the image encoder-decoder pair (such as VQVAE or VQGAN), and  $d$  is the dimensionality of these features. As the text tokenization, since the image tokens represent indices in the codebook  $\mathcal{C}$ , each image token  $x_{N+i}$  maps to  $c_{x_{N+i}}$ , which is then rearranged into a  $h \times w \times d$  shaped tensor in raster-scan order (from top-left to bottom-right), for  $h = H/f$  and  $w = W/f$  when  $f$  is down-sampling factor. After that, rearranged latent is fed into the image decoder  $D: \mathbb{R}^{h \times w \times d} \rightarrow \mathbb{R}^{H \times W \times C}$  to construct an actual RGB image.

## A.2 SPECULATIVE DECODING

**Draft phase** Given a sequence of tokens  $X_{1:N} = (x_1, \dots, x_N)$ , the drafter model generates  $\gamma$  draft tokens  $\hat{X}_{1:\gamma}$  as speculations for the next  $\gamma$  tokens following  $X_{1:N}$ , based on the drafter distribution  $p$ . Each draft token  $\hat{x}_i$  is sampled from the drafter distribution  $p(\hat{x}_i | (X_{1:N}, \hat{X}_{1:i-1}))$  for each  $i = 1, \dots, \gamma$ , thus requiring  $\gamma$  steps to generate  $\gamma$  draft tokens.

**Verification phase** After obtaining the draft tokens, the concatenated sequence  $(X_{1:N}, \hat{X}_{1:\gamma})$  is fed into the target model, which calculates the likelihood of each draft token  $q(\hat{x}_i | (X_{1:N}, \hat{X}_{1:i-1}))$  in parallel within a single forward pass. Each draft token  $\hat{x}_i$  is accepted with a probability:

$$\min \left( 1, \frac{q(\hat{x}_i | (X_{1:N}, \hat{X}_{1:i-1}))}{p(\hat{x}_i | (X_{1:N}, \hat{X}_{1:i-1}))} \right). \quad (1)$$

If  $\hat{x}_i$  is accepted, it is immediately set as  $x_{N+i} = \hat{x}_i$ . Otherwise, all subsequent tokens  $\hat{X}_{i+1:\gamma}$  are discarded, and  $x_{N+i}$  is resampled from a distribution defined by  $[q(\cdot | (X_{1:N}, \hat{X}_{1:i-1})) - p(\cdot | (X_{1:N}, \hat{X}_{1:i-1}))]_+$ , where  $[\cdot]_+$  denotes normalization over positive values only. As proven by [Leviathan et al. \(2023\)](#), this approach ensures that the distribution of the generated token sequence matches the distribution produced by the target model.

**Tree drafting and decoding** The standard draft and verification phases typically rely on chain drafting (i.e., a single token sequence). However, Medusa ([Cai et al., 2024](#)) and EAGLE ([Li et al., 2024a;b](#)) introduce a tree structure for draft tokens that significantly improves step compression. Below, we briefly overview tree drafting and its verification.

In tree drafting, each forward pass produces multiple tokens, forming a tree. Given a sequence  $X_{1:N}$ , the drafter generates  $s_1$  tokens  $\hat{x}_{1,1}, \dots, \hat{x}_{1,s_1}$  in one pass; for each  $\hat{x}_{1,i}$ , it then generates another  $s_2$  tokens  $\hat{x}_{2,i,1}, \dots, \hat{x}_{2,i,s_2}$ , and so on, until a limit or maximum depth is reached. A tree-aware attention mask ensures that generating all these tokens still requires only one forward pass per layer of the tree by masking out non-ancestor nodes. Thus, a depth- $K$  tree—containing many more tokens than a chain—can still be built with just  $K$  passes.

Tree drafting can be categorized into static tree-based drafting, where the tree structure is predetermined and consistently used, and dynamic tree-based drafting, where the tree structure is dynamically determined based on the drafter’s confidence. In LLMs, dynamic tree drafting leverages a well-calibrated drafter to effectively find tree structures that increase the acceptance length, leading to significant speed improvements over static tree-based drafting without requiring additional training for the drafter.

For verification, the draft tree is flattened into a single sequence and fed into the target model with a matching tree-aware mask, allowing verification in a single pass. By widening the range of draft tokens, tree drafting increases the probability of accepting more tokens overall.

## B EXPERIMENTAL DETAILS

**Models.** The evaluation is conducted on three recent visual AR models: LlamaGen (Sun et al., 2024), Anole (Chern et al., 2024), and Lumina-mGPT (Liu et al., 2024). For LlamaGen, we use the text-conditioned LlamaGen-XL (775M) Stage I and II models, which generate images at resolutions of  $256 \times 256$  and  $512 \times 512$ , respectively. Anole is a 7B parameter model that generates  $512 \times 512$  images, while Lumina-mGPT is evaluated with the Lumina-mGPT-7B-768 variant, which has 7B parameters and generates images at  $768 \times 768$  resolution. In line with EAGLE (Li et al., 2024a;b), each model uses a single decoder layer as the drafter model: a LlamaDecoderLayer for LlamaGen and ChameleonDecoderLayer for both Anole and Lumina-mGPT, with internal dimensionalities matching their respective target models. Note that classifier-free guidance scale is set to be 3.0 and temperature 1.0 and top- $k$  sampling with  $k = 2000$  is applied for all experiments unless otherwise specified.

**Drafter Training.** For training the drafter model for LlamaGen, we randomly sample 100K images from the LAION-COCO dataset (Chuhmann et al., 2022). For Anole and Lumina-mGPT, we generate 118K and 30K images using the target model each, based on the captions randomly sampled from the train set of MS-COCO 2017 (Lin et al., 2014). The training procedure is adapted from EAGLE with minor adjustments to accommodate the presence of classifier-free guidance (Ho & Salimans, 2021), with a 0.9 probability of selecting text-conditioned samples and a 0.1 probability for null-conditioned samples. AdamW (Loshchilov & Hutter, 2019) is used as the optimizer with a learning rate  $1.0 \times 10^{-4}$ , a batch size of 16, and a total of 20 training epochs.

**Metrics and Benchmark.** For evaluating acceleration performance, we measure the step compression ratio  $\mathcal{S} = \frac{\# \text{generated tokens}}{\# \text{decoding steps}}$  (Fu et al., 2024), and the actual speed up in terms of latency. Latencies are measured on a highly controlled system to minimize non-intended sources of latency. Specifically, we use batch size 1 on a single A100 PCIe 80GB GPU, with all implementation factors kept constant except for the algorithm. To assess visual quality, we employ Fréchet inception distance (FID) (Heusel et al., 2017) and CLIP Score (Hessel et al., 2021). The validation set of MS-COCO 2017 (Lin et al., 2014) and Parti prompts (Yu et al., 2022) serve as benchmark datasets. For the Parti prompts, only the CLIP Score is reported, as ground truth images are not available.

**Static Tree Structures.** To ensure a fair comparison with EAGLE-2, which employs dynamic tree drafting with 59 nodes, we extend the static tree structure of EAGLE-1 to include 58 nodes, maintaining a comparable scale. The extension preserves the macroscopic structure of EAGLE-1 while incorporating additional branches to improve depth and coverage. Following EAGLE-1’s design philosophy, we allocate more nodes to the left branches, prioritizing early-stage expansions where acceptance probabilities tend to be higher. As shown in Figure 3, this extended static tree structure is used for both EAGLE-1 and LANTERN++ in our experiments to ensure consistency in static tree-based drafting.

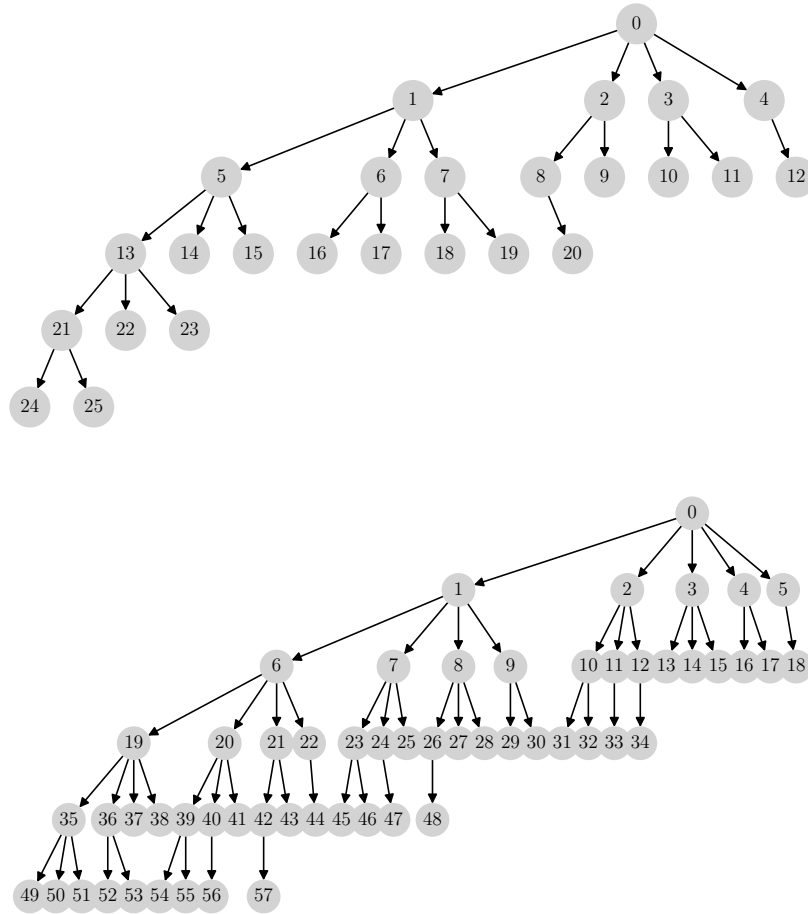


Figure 3: Comparison of static tree structures. **Top:** The original static tree used in EAGLE-1. **Bottom:** The extended static tree used for both EAGLE-1 and LANTERN++ in our experiments, designed to match the scale of dynamic tree drafting while maintaining EAGLE-1’s structural principles.

## C ADDITIONAL EXPERIMENTAL RESULTS

### C.1 AN EXAMPLE OF SHALLOW DYNAMIC TREE

Due to token selection ambiguity, dynamic tree drafting often results in a shallow and unbalanced draft tree. As discussed in Section 3, low drafter confidence causes long token sequences to have significantly lower global accept probabilities, leading to a bias toward shorter sequences. Figure 4 illustrates an example tree obtained from dynamic drafting, where most branches remain short, and deeper expansions are rarely selected. This confirms our earlier observation that dynamic tree drafting struggles to construct long accepted sequences, ultimately limiting its acceleration potential.

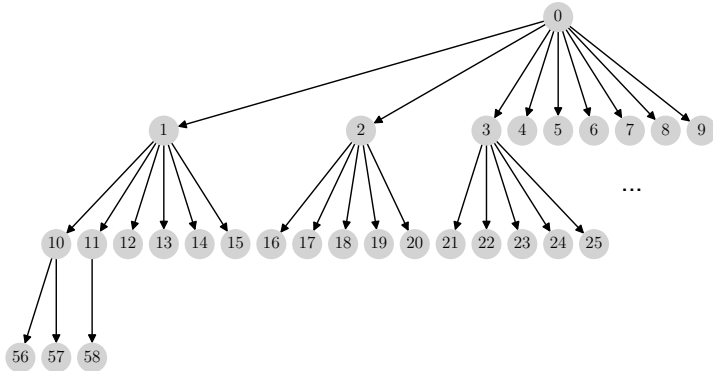


Figure 4: Example of a shallow draft tree produced by dynamic tree drafting. Due to low drafter confidence, deeper expansions are rarely selected, resulting in a tree that is wide but lacks depth, which hinders step compression.

### C.2 COMPARING ADDITIVE AND MULTIPLICATIVE RELAXATION

Table 3: Step compression ratios achieved with different values of  $\lambda$  and  $\delta$ . Multiplicative relaxation ( $\lambda$ ) provides a consistent increase across all settings, whereas additive relaxation ( $\delta$ ) exhibits a more gradual improvement due to its uneven effect on tokens with varying probabilities. Results are averaged over 100 randomly sampled captions from the MS-COCO 2017 validation set.

| Multiplicative Relaxation ( $\lambda$ ) |                    |                             |                             |
|---|--------------------|-----------------------------|-----------------------------|
| <b>EAGLE-1: 2.81</b>                    | $\lambda = 5$      | $\lambda = 10$              | $\lambda = 20$              |
| $k = 5$                                 | 3.02               | 3.17                        | 3.30                        |
| $k = 10$                                | 3.13               | 3.39                        | 3.59                        |
| $k = 20$                                | 3.42               | 3.82                        | 3.95                        |
| $k = 50$                                | 3.68               | 4.13                        | 4.46                        |
| Additive Relaxation ( $\delta$ )        |                    |                             |                             |
| <b>EAGLE-1: 2.81</b>                    | $\delta = 10^{-4}$ | $\delta = 2 \times 10^{-4}$ | $\delta = 5 \times 10^{-4}$ |
| $k = 5$                                 | 2.87               | 2.93                        | 3.07                        |
| $k = 10$                                | 2.83               | 2.96                        | 3.35                        |
| $k = 20$                                | 2.90               | 3.05                        | 3.51                        |
| $k = 50$                                | 2.92               | 3.15                        | 3.69                        |

To evaluate the effectiveness of different relaxation mechanisms in speculative decoding, we compare multiplicative ( $\lambda$ ) and additive ( $\delta$ ) relaxation in terms of acceleration and image quality. Table 3 shows the step compression ratios achieved with varying values of  $k$ ,  $\lambda$ , and  $\delta$ . While both methods improve acceleration, a key distinction emerges:  $\lambda$  leads to a more consistent increase across all settings, whereas  $\delta$  exhibits a more gradual improvement with less variation.

This discrepancy arises from how each method interacts with the underlying probability distribution. In multiplicative relaxation, the acceptance probability is scaled in proportion to the original target probability  $q(x|s)$ , ensuring that the increase remains relative to the inherent confidence of the target model. This leads to *a stable and uniform acceleration gain*, as every token benefits from a proportional probability boost.

In contrast, additive relaxation applies a fixed probability shift, which interacts differently with tokens of varying probabilities. When a token has a low likelihood, the additive increase has a strong impact, whereas for higher-probability tokens, the effect is relatively weak. Since token probabilities in visual AR models are highly dispersed due to token selection ambiguity, this results in *an uneven relaxation effect across different tokens*. Consequently,  $\delta$  exhibits a more constrained step compression improvement, with some tokens receiving insufficient probability adjustment.

The impact of these differences is also visible in image quality, as shown in Figure 5. While both relaxation strategies maintain reasonable fidelity at lower values, additive relaxation introduces more inconsistencies as  $\delta$  increases. This effect is likely due to uneven probability adjustments leading to local distortions, particularly for tokens that receive disproportionately large or small probability shifts. In contrast, multiplicative relaxation maintains a consistent probability scaling across different token types, resulting in more stable image quality while achieving higher step compression.

Overall, our results suggest that while both approaches can improve speculative decoding efficiency, multiplicative relaxation is better suited for static tree drafting. By ensuring a controlled proportional increase, it provides a predictable balance between acceleration and image preservation, making it a preferable choice for visual AR models.

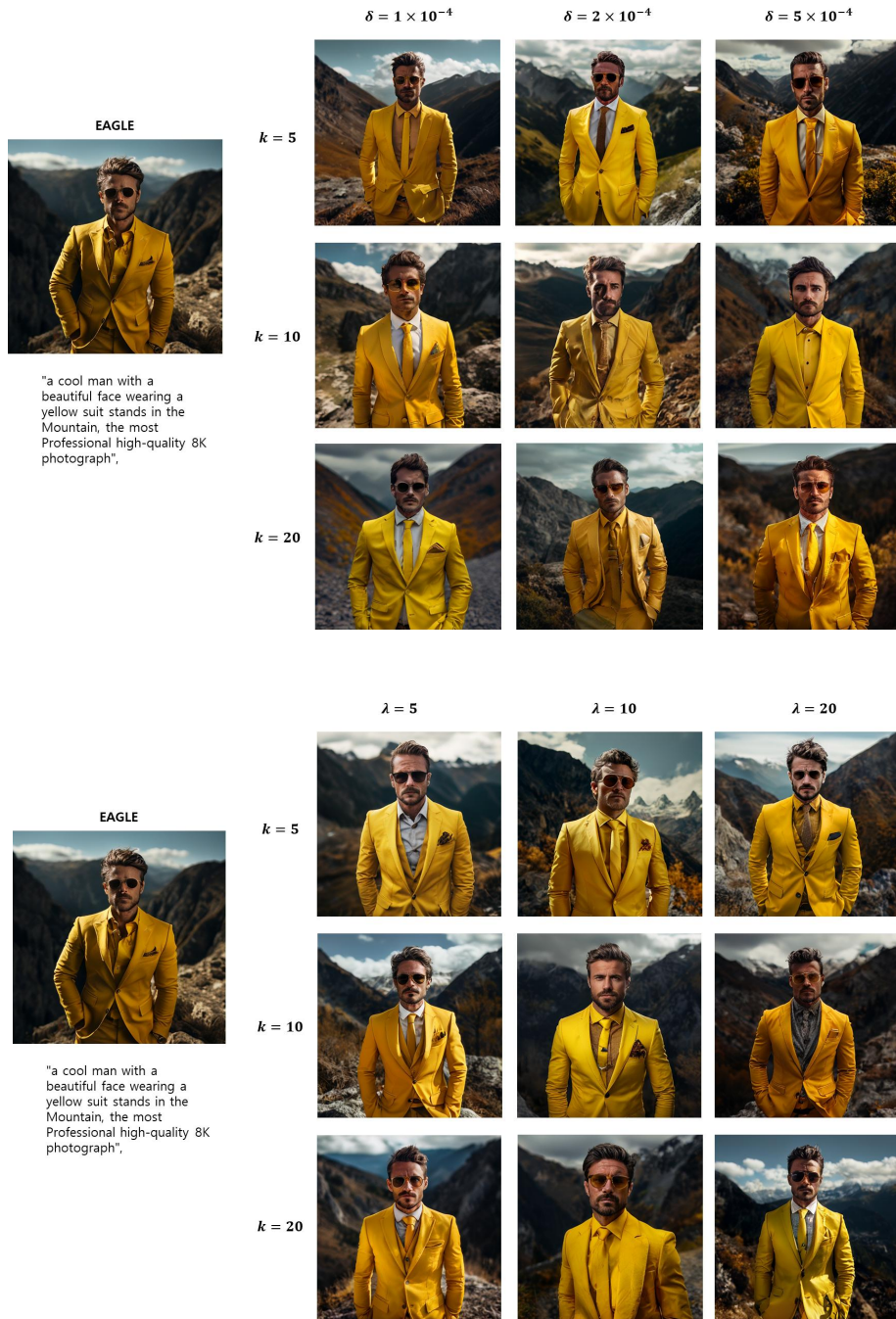


Figure 5: Comparison of images generated using additive relaxation ( $\delta$ ) and multiplicative relaxation ( $\lambda$ ). The left column shows images generated without relaxation. The middle and right columns show images with increasing levels of  $\delta$  and  $\lambda$ , respectively. While both approaches increase acceleration, additive relaxation leads to more noticeable artifacts, whereas multiplicative relaxation maintains stable image quality.

Table 4: Step compression ratio comparison between the original and extended static tree. The extended tree consistently improves acceleration across all settings.

| <b>Original (N=26)</b> | $\lambda = 5$ | $\lambda = 10$ | $\lambda = 20$ |
|------------------------|---------------|----------------|----------------|
| $k = 5$                | 3.02          | 3.17           | 3.30           |
| $k = 10$               | 3.13          | 3.39           | 3.59           |
| $k = 20$               | 3.42          | 3.82           | 3.95           |
| $k = 50$               | 3.68          | 4.13           | 4.46           |
| <b>Extended (N=58)</b> | $\lambda = 5$ | $\lambda = 10$ | $\lambda = 20$ |
| $k = 5$                | 3.28 (+0.26)  | 3.33 (+0.16)   | 3.52 (+0.22)   |
| $k = 10$               | 3.51 (+0.39)  | 3.78 (+0.39)   | 3.83 (+0.24)   |
| $k = 20$               | 3.63 (+0.19)  | 4.03 (+0.21)   | 4.24 (+0.29)   |
| $k = 50$               | 3.91 (+0.23)  | 4.32 (+0.19)   | 4.64 (+0.18)   |

Table 5: Latency comparison between the original and extended static tree. The extended tree reduces inference time across most settings despite the increase in context length.

| <b>Original (N=26)</b> | $\lambda = 5$   | $\lambda = 10$  | $\lambda = 20$  |
|------------------------|-----------------|-----------------|-----------------|
| $k = 5$                | 76.53s          | 73.18s          | 70.44s          |
| $k = 10$               | 74.26s          | 68.69s          | 65.05s          |
| $k = 20$               | 68.06s          | 61.43s          | 59.59s          |
| $k = 50$               | 63.17s          | 56.51s          | 52.69s          |
| <b>Extended (N=58)</b> | $\lambda = 5$   | $\lambda = 10$  | $\lambda = 20$  |
| $k = 5$                | 73.50s (-3.03s) | 72.69s (-0.51s) | 68.83s (-1.61s) |
| $k = 10$               | 68.86s (-5.40s) | 64.67s (-3.98s) | 63.23s (-1.82s) |
| $k = 20$               | 66.97s (-1.09s) | 60.54s (-0.89s) | 57.24s (-2.35s) |
| $k = 50$               | 62.36s (-0.81s) | 56.03s (-0.48s) | 52.06s (-0.63s) |

### C.3 IMPACT OF EXTENDED STATIC TREE ON ACCELERATION AND LATENCY

To further improve the acceleration performance of speculative decoding under static tree drafting, we investigate the effect of using an extended static tree with a deeper structure, as illustrated in Figure 3. The goal of this extension is to increase the number of draft tokens per step while preserving a balanced trade-off between acceleration and computational efficiency. Tables 4 and 5 present the comparison of step compression ratios and latency between the original and extended static tree structures.

The results indicate that increasing the tree depth significantly enhances the step compression ratio. The original static tree ( $N = 26$  nodes) achieves a maximum compression of  $\times 4.46$  under  $\lambda = 20, k = 50$ , whereas the extended static tree ( $N = 58$  nodes) further improves it to  $\times 4.64$ , demonstrating a consistent advantage across all  $\lambda$  and  $k$  settings. Notably, the most pronounced improvements occur at moderate  $k$  values (e.g.,  $k = 10$  and  $k = 20$ ), suggesting that the extended tree structure provides additional opportunities for token acceptance while maintaining stability in token predictions.

Latency analysis in Table 5 reveals that despite generating a larger number of draft tokens, the extended static tree *does not introduce significant computational overhead*. In fact, it reduces overall inference latency across most configurations, with improvements reaching up to 5.40 seconds for  $k = 10, \lambda = 5$ . This suggests that the extended tree structure facilitates speculative decoding by reducing the number of autoregressive decoding steps, thereby lowering the required target model evaluations.

An important consideration is that increasing the number of nodes in draft tree inherently leads to a longer context length during verification, which can introduce computational overhead. However, our results show that despite this potential drawback, the extended static tree consistently achieves

faster inference. This improvement arises because the additional draft tokens allow more aggressive speculative decoding, effectively compensating for the increased context length. The reduction in required target model calls outweighs the cost of handling a longer context, leading to an overall speedup.

One interesting observation is that while larger  $\lambda$  values offer higher step compression, their impact on latency reduction diminishes at higher values (e.g.,  $k = 50, \lambda = 20$ ). This suggests that while the extended static tree allows for deeper draft sequences, the overall limits of speculative decoding still impose an upper bound on achievable acceleration.

Overall, these results demonstrate that increasing tree depth is an effective strategy for further improving speculative decoding in visual AR models. The extended static tree structure enables higher step compression and lower latency, making it a promising approach for optimizing inference speed in visual AR generation.